Nanotechnology **23** (2012) 255705 (7pp) doi:10.1088/0957-4484/23/25/255705

Electrodeposition of gold thin films with controlled morphologies and their applications in electrocatalysis and SERS

Jamil Elias[1], Magdalena Gizowska[2,3], Pierre Brodard[1], Roland Widmer[4], Yoram deHazan[2], Thomas Graule[2], Johann Michler[1] and Laetitia Philippe[1]

[1] EMPA—Materials Science and Technology, Laboratory for Mechanics of Materials and Nanostructures, Swiss Federal Laboratories for Materials Testing and Research, Feuerwerkstrasse 39, CH-3602 Thun, Switzerland
[2] EMPA—Materials Science and Technology, Laboratory for High Performance Ceramics, Swiss Federal Laboratories for Materials Testing and Research, Ueberlandstrasse 129, CH-8600 Duebendorf, Switzerland
[3] Faculty of Chemistry, Warsaw University of Technology, ulica Noakowskiego 3, PL-00-664 Warszawa, Poland
[4] EMPA—Materials Science and Technology, nanotech@surfaces Laboratory, Swiss Federal Laboratories for Materials Testing and Research, Ueberlandstrasse 129, CH-8600 Duebendorf, Switzerland

E-mail: jamil.elias@empa.ch

Received 12 December 2011, in final form 8 May 2012
Published 31 May 2012
Online at stacks.iop.org/Nano/23/255705

Abstract
Here, an easy and effective electrochemical route towards the synthesis of gold thin films with well-controlled roughness, morphology and crystallographic orientation is reported. To control these different factors, the applied potential during deposition played a major role. A tentative nucleation and growth mechanism is demonstrated by means of electrochemical characterizations and a formation mechanism is proposed. Interestingly, the differences in geometry and orientation of the different gold deposits have shown a clear correlation with the electrocatalytical activity in the case of oxygen sensing. In addition, not only the electrocatalytical activity but also the surface-enhanced Raman scattering of the gold deposits have been found to depend both on the roughness and on the size of the surface nanostructures, allowing a fine tuning by controlling these two parameters during deposition.

(Some figures may appear in colour only in the online journal)

1. Introduction

Nanostructured noble metals have progressively attracted attention due to their interesting optical [1], electrochemical [2], electronic [3] and photoelectrochemical properties [4]. Among these metals, gold is of special importance due to its stability and unique optical properties [5]. Therefore, a lot of effort has been dedicated to gold nanostructures, mainly due to their exciting applications as substrates for surface-enhanced Raman scattering (SERS) [6], superhydrophobicity [7], catalysis [8] or sensors [9]. The morphology of gold surfaces, especially the roughness, is the main parameter that influences their functional properties. This is of particular importance for SERS [10] and superhydrophobicity applications [7], where the signal enhancement factor and the contact angle are directly related to the nanoscale morphology. The catalytic activity of metal nanostructures [11] can also be controlled easily by tuning their shape, and gold nanostructures with defined surface roughness and morphology may also find several technological applications as selective solar absorbers, antireflection coatings or diffraction gratings [12].

Nanostructured gold films are often prepared by methods based on high vacuum, such as sputtering [13], evaporation [14] and molecular beam epitaxy (MBE) [15]. In addition, in these relatively high cost processes, the control of roughness and shape of the obtained gold deposits is still poor. As an alternative synthesis technique, electrodeposition is commercially the most important process because of its time efficiency, cost effectiveness and absence of vacuum technology. It also allows changes in the grain size and deposition layer thickness by varying the deposition rate. Many approaches have been employed to synthesize gold layers with different shapes by electrochemical deposition [16–18]. However, in order to control the morphology and the roughness of the gold electrodeposits, most of these approaches require the presence of additives in the electrochemical bath and/or a pretreatment of the conductive substrate, which increases the production costs [19]. For example, Tian *et al* [17] have reported the electrodeposition of gold nanostructures with different morphologies (pyramidal, rod-like and spherical) by varying the applied potential and the concentration of gold precursor in the electrochemical bath. However, an additional pretreatment step consisting of a sputtering of the gold layer on a TCO substrate has to be done to obtain such structures.

In this paper we report on a simple one-step electrodeposition approach to synthesize gold structures with controlled roughness and morphology on a clean substrate without introducing any additives. The morphology and the roughness of the gold deposits can be easily controlled by varying the applied deposition potential and the charge density in a timescale compatible with large-scale production. Based on the experimental results and electrochemical characterizations, the growth mechanism will be discussed.

2. Experimental procedure

Gold nanostructures were prepared on transparent conductive oxide glass substrates (TCO, glass/SnO_2:F, 10 Ω/sq, Solaronix) by means of electrochemical deposition from an aqueous gold bath containing 10 g l^{-1} of $K[Au(CN)_2]$ and 100 g l^{-1} of KH_2PO_4 at 55 °C. The ultrapure water (18 MΩ cm) was provided by an Elga set-up. Before electrodeposition, the bare TCO was cleaned thoroughly by sonication in acetone, ethanol and isopropanol, consecutively, for 15 min each. The cleaned TCO was then used as a working electrode in a three-electrode electrochemical cell, with a Pt spiral wire as the counter electrode and an Ag/AgCl (saturated KCl) reference electrode. The applied deposition potential was in the range of −0.7 to −1.2 V and the total charge density passed through the cell during the film growth was from 0.05 to 2.5 C cm^{-2}. During electrodeposition experiments, the solution was stirred at 300 rpm.

Voltamperometry experiments were performed on a glass/SnO_2:F substrate with the same conditions (temperature and solution) used for the electrochemical deposition. Two scans for each solution were carried out from rest potential (near zero), with a cathodic sweep to −1.3 V followed by an anodic sweep to −0.2 V. Only the cathodic sweeps are shown for the sake of clarity. The scan rate was set to 50 mV s^{-1}. The solutions were deaerated 10 min before and during the experiments with argon to minimize the amount of dissolved oxygen. A geometric surface of 0.36 cm^2 was masked off prior to the experiments. Voltamperometry and electrodeposition experiments were performed using a MicroAutolab type III potentiostat. The morphology of the samples was observed by scanning electron microscopy (SEM, Hitachi S-4800).

Atomic force microscopy (AFM) experiments were carried out in tapping mode to decrease tip–substrate interactions and were performed with a commercial AFM/STM Nanoscope III Multimode (Veeco) using ultrasharp silicon cantilevers (NT-MDT) with a typical curvature radius of 6 nm. AFM data were analysed using WSxM software [20].

Raman spectra were recorded with a reflective-type micro-Raman spectrometer (Renishaw Ramascope) equipped with a HeNe laser operating at 632.8 nm as the excitation source (laser power ∼ 0.25–0.5 mW, 100× objective, laser spot diameter ∼ 1 μm). In order to test the SERS response of the samples, we drop-coated a [10^{-7} M] solution of Brilliant Cresyl Blue ($C_{17}H_{20}N_3OCl{\cdot}1/2ZnCl_2$, BCB) in EtOH. The acquisition time for each spectrum was 0.1 s and each measurement was repeated four times at four different locations. All spectra are baseline-corrected.

3. Results and discussion

3.1. Morphology

Figure 1 shows the SEM images of the gold deposits obtained by passing a constant charge density (1 C cm^{-2}) at different applied deposition potentials (from −0.7 to −1.2 V) on clean TCO substrates. All the other parameters (temperature, concentration, etc) were kept constant. As can be seen in figure 1, gold deposits with different shapes and sizes have been obtained. The deposition at the lowest applied potential (−0.7 V, figure 1(a)) produced a large number of overlapping crystals with micrometre size and polyangular shape. A compact layer of gold was also obtained at −0.8 V (figure 1(b)) but here the deposit consists of particles with nanometre size. By cathodically increasing the potential to −0.9 V, two growing phases were revealed from the SEM micrograph in figure 1(c). In other terms, platelet-like nanostructures (inset of figure 1(c)) started to appear simultaneously with a similar nanocrystalline layer observed previously at −0.8 V (figure 1(b)). The platelet-like nanostructures increased in size and density and transformed into tetragonal pyramidal shape when the applied deposition potential reaches −1 V (figure 1(d)). When the applied potential reaches −1.1 V, the deposit became more uniform and was completely constituted by the tetragonal pyramidal shaped nanostructures (figure 1(e)). By further cathodically increasing the potential to −1.2 V, the size of these nanostructures increases (figure 1(f)).

More positive than −0.7 V, separated gold microparticles with angular shape have been obtained (not shown here). On the other hand, by shifting the potential below −1.3 V, the

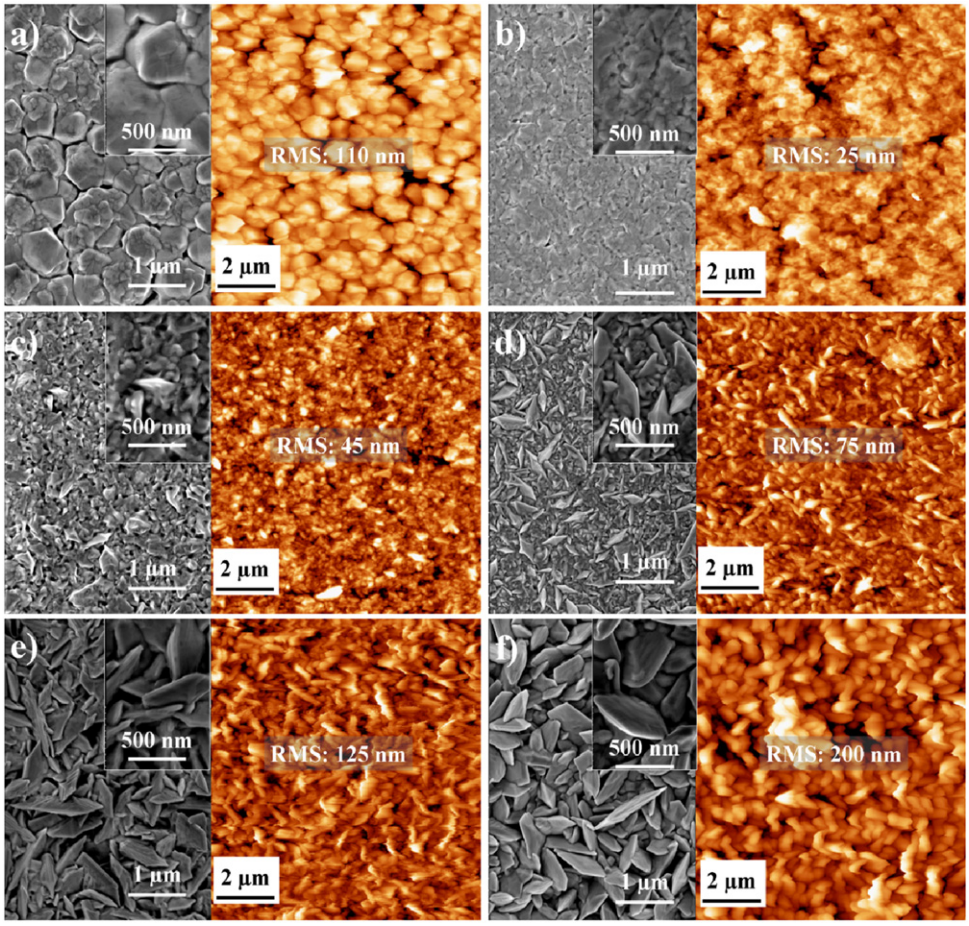

Figure 1. SEM and AFM images of the Au thin films with different applied potentials and roughnesses: (a) −0.7 V, (b) −0.8 V, (c) −0.9 V, (d) −1 V, (e) −1.1 V and (f) −1.2 V. The AFM images are shown on the right of each SEM image.

gold deposit delaminates rapidly from the substrate during the electrodeposition process. This might be due to the stress induced in the deposit during such a fast growth process. Interestingly, visual inspection showed that the surface of deposits passed gradually from yellow-bright to brown-matt when the applied deposition potential was increased from −0.7 to −1.2 V. This is probably related to the surface roughness and the particle size [21]. The roughnesses of the obtained deposits were analysed by AFM and the results are depicted in figure 1 (right side of each SEM image). The mean surface roughness was 110 nm in the case of −0.7 V, then it decreases to a minimum (25 nm) for −0.8 V and increases linearly as a function of potential to reach 200 nm for −1.2 V. This shows that the mean surface roughness of the gold layers can be very precisely controlled by controlling the electrochemical synthesis conditions.

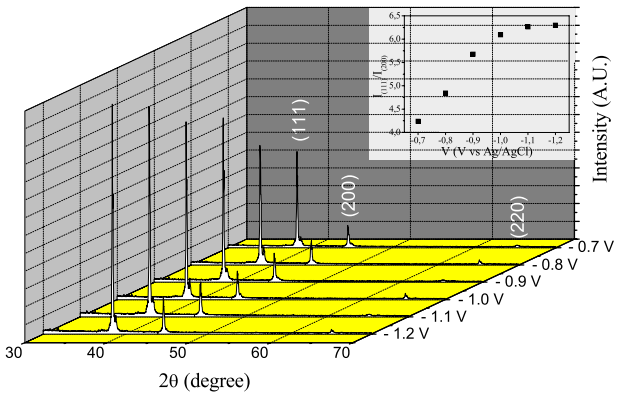

Figure 2. XRD patterns of gold deposits obtained at different applied potentials as well as their relative peak intensities (inset) corresponding to the (111) and (200) planes ($I(111)/I(200)$).

3.2. Microstructures and compositions

The crystalline nature of the phase and its purity were determined by XRD. Representative XRD patterns of the as-obtained products are shown in figure 2 in the 2θ range of 30°–70°.

The characteristic peaks of the as-prepared products arise at $2\theta = 38.2°$, 44.5°and 64.7° which matches the reflection planes of (111), (200) and (220), respectively. All the diffraction peaks can be well indexed to the face-centred cubic (fcc) structure of metallic Au with the space group $Fm\bar{3}m$, which is consistent with the standard values reported in JCPDS, card no. 04-0784. In addition, the relative intensities of the peaks corresponding to the (111) and (200) planes ($I_{(111)}/I_{(200)}$) are for all synthesis conditions significantly

higher (see the inset of figure 2) than the standard value described in the JCPDS card (1.9), which indicates that the preferred growth orientation of the products is the [111] direction. Importantly, the gold deposits are more and more oriented in this direction when the applied deposition potential increases. No characteristic peaks due to other phases are detected, indicating that the as-prepared products obtained by the present synthetic route consist of a pure phase. Furthermore, EDX analyses have been carried out on the different gold deposits and no impurities have been detected.

3.3. Voltamperometry study

In order to understand the morphology changes at different applied deposition potentials, a voltamperometry study has been carried out. Figure 3 shows two polarization curves recorded at 50 mV s^{-1} and obtained by using the same conditions (temperature, concentration, etc) used for the electrodeposition of gold with (dashed curve) and without (solid curve) $KAu(CN)_2$. Only the cathodic forward sweeps are shown for the sake of clarity. In the case of the solution containing the gold precursor, the second polarization scan was chosen because a gold deposit was expected to cover the TCO substrate during the first scan. For the curve recorded without $KAu(CN)_2$, the cathodic current density decay began at a negative potential of about −0.9 V, which is attributed to the hydrogen evolution reaction (HER) in the aqueous solution. During the measurement, hydrogen bubbles were observed on the cathode surface at about −1 V. The absence of other cathodic threshold potentials indicates that KH_2PO_4 is electrochemically inactive [22]. The dashed CV curve recorded with the solution used for the gold synthesis (KH_2PO_4 and $KAu(CN)_2$) shows three different parts (coloured areas in the polarization curves). In the first part, a small increase of the current density followed by a large peak between −0.3 and −0.6 V was detected. Li *et al* [23] have studied the electrodeposition of gold on a copper substrate and demonstrated that such a peak in this potential range was attributed to the adsorption of gold cyanide on the electrode. The second part of the curve, between −0.6 and −0.9 V, shows a constant current density. During the cathodic sweep recorded in the first scan, gold deposition was observed on the TCO substrate when the potential reached −0.6 V, which means that the electrochemical reaction for gold electrodeposition starts from this potential. Bindra *et al* [24] showed that, in this range of potentials (part 2), gold deposits have been obtained from the reduction of AuCN adsorbed on the cathode surface, rather than from the direct reduction of $Au(CN)_2^-$ by charge transfer reaction directly from the solution. Therefore, at this step the electrodeposition follows the following sequence of reactions [25]:

$$(AuCN)_{solution} \rightarrow (AuCN)_{ads} \quad (1)$$

$$(AuCN)_{ads} + e^- \rightarrow (AuCN^-)_{ads} \quad (2)$$

$$(AuCN^-)_{ads} + H^+ \rightarrow Au + HCN. \quad (3)$$

At more negative potentials, in part 3 of the CV curve, when the current density increases abruptly, the electrochemical

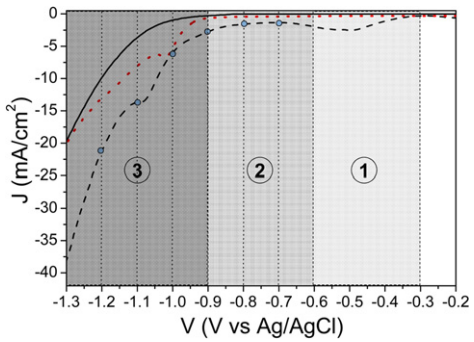

Figure 3. Cyclic voltammograms obtained on TCO substrate in aqueous solutions of KH_2PO_4 (solid curve) or $K[Au(CN)_2]$ and KH_2PO_4 (dotted curve: first scan and dashed curve: second scan). Only cathodic sweeps are shown for the sake of clarity.

deposition of gold was governed by the following direct charge transfer reaction [25]:

$$AuCN_2^- + 2H^+ + e^- \rightarrow Au + 2HCN. \quad (4)$$

Furthermore, according to the results without $KAu(CN)_2$ mentioned above, this region is also governed by the hydrogen evolution reaction (reduction of water). Consequently, a clear current density shoulder can be seen around −1.1 V, proving the coexistence in this region of two competing electrochemical processes: direct charge transfer and hydrogen evolution reactions.

A clear correlation can be identified by comparing the gold deposits obtained in figure 1 and the dashed polarization curve in figure 3. For deposits obtained in the second potential range of the polarization curves (−0.6 to −0.9 V), the gold morphology was compact and uniform irrespective of the grain size which was decreased by increasing the applied potential (figures 1(a) and (b)). In the transition potential (between parts 2 and 3), when the hydrogen evolution and direct charge transfer mechanisms start to take place, two growing phases were obtained as can be seen at −0.9 V in figure 1(c). In part 3, when the current density increased significantly, the platelet-like structures are transformed to tetragonal pyramidal shapes at −1 V and completely covered the substrate once the potential reached −1.1 V. We conclude that the competition between the hydrogen evolution and the direct charge transfer reactions is the main reason for obtaining tetragonal shaped structures.

3.4. Chronoamperometric characterization

In order to gain a better understanding of the growth of the nanostructured layers obtained at higher potentials, the evolution of the morphology as a function of charge density (deposition time) was studied by SEM. For this study, the applied potential was fixed at −1.2 V.

Figure 4 shows the *J–t* curve in parallel to the morphology variation at different deposition times. The charge density values (between 0.05 and 2.5 C cm^{-2}) have been chosen in order to correspond to the different parts of the

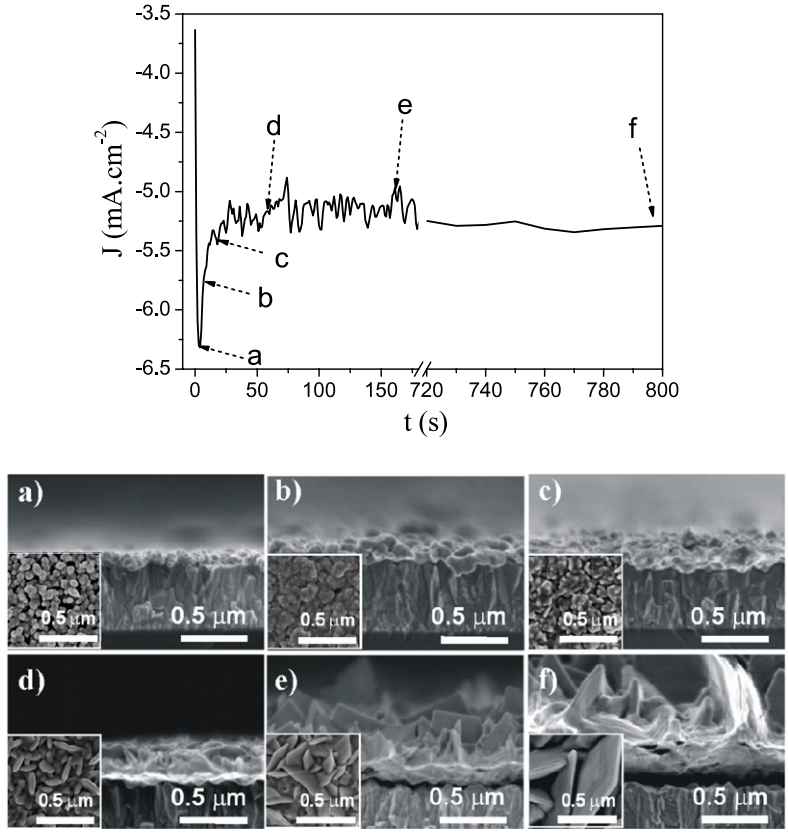

Figure 4. Current–density–time curve recorded during gold electrodeposition at −1.2 V. The cross-sectional SEM images correspond to the different gold deposits obtained at different electrodeposition times from the current–density–time curve. The lower left inset of each cross-sectional image corresponds to its high magnification SEM image top view.

J–t curve. At 0.05 C cm^{-2}, when the current density reaches the minimum ((a) in figure 4), nanoparticles with sizes of about 50 nm covering uniformly the TCO substrate have been obtained.

These nanoparticles increase in size and coalesce with each other in the bulk part of the layer during the increase of the current density (0.1 C cm^{-2}, figure 4(b)) while keeping almost the same particle density as the one obtained with the previous sample (figure 4(a)). When the current density reaches the transition point before the plateau (0.175 C cm^{-2}, (c) in figure 4), small platelet-like nanostructures start to grow.

The surface was completely uniform and covered by the nanosized platelets (∼50 nm) in a relatively short deposition time (∼50 s, corresponding to 0.25 C cm^{-2}, d in figure 4). By comparing the cross sections of the last two deposits (figure 4(c) and (d)) we can see that the thicknesses from the bottom (∼130 nm), constituted by compact layers, do not change significantly during the growth time: only the platelet structures increase in size and density. By increasing even more the synthesis time (0.5 C cm^{-2}), the platelets are increased in size and transformed to tetragonal pyramids after a while (e.g. 1 and 2.5 C cm^{-2}, see figures 4(e) and (f), respectively). It is important to note that here also the thickness of the lower part (compact layer) is still almost constant during the time of deposition.

3.5. Overall nucleation and growth mechanism

As we have seen earlier in this paper, at −1.2 V, the deposition process is governed by hydrogen evolution and direct charge transfer reactions. Therefore, the hydrogen bubbles generated after the first growth stage might be the cause of the inhibition of growth on some random distributed sites on the gold surface. As a result, the platelet nanostructures are generated during the first growth stage on the active sites between the hydrogen bubbles. For this reason, the gold anions diffuse from the solution and reduce on the most accessible sites of gold (the platelet) obtained in the first growth stage, to give finally the tetragonal pyramidal structures.

Based on the SEM results and the electrochemical characterizations, a schematic illustration of the formation mechanism of gold is presented in figure 5.

3.6. Electrocatalytic activity and SERS

As a first application, we investigated the electrocatalytic activity by studying the oxygen reduction reaction on the nanostructured gold surfaces. This reaction is an important process in fuel cells, chemical sensing and other electrochemical technologies and its kinetics has been widely studied [26]. Furthermore, the reaction pathway is highly dependent on the geometry and the crystallographic

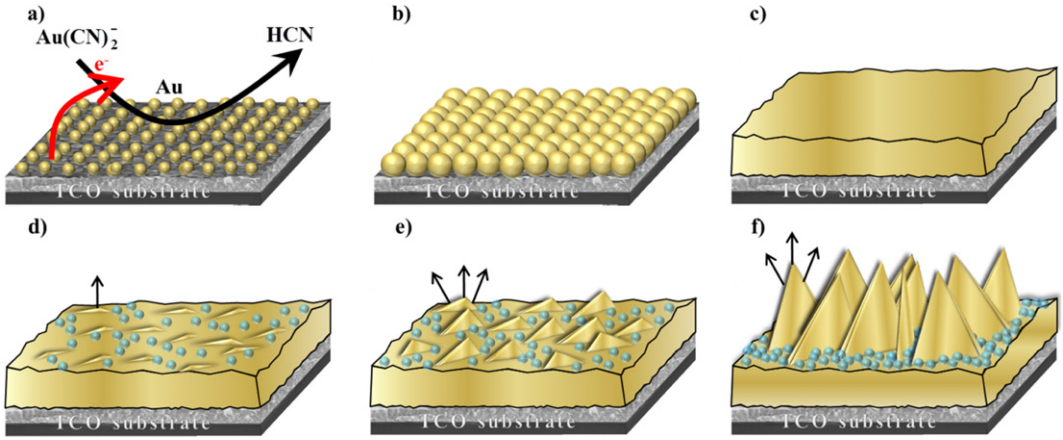

Figure 5. Schematic view of the proposed nucleation and growth mechanism for the electrodeposition of rough gold thin layers.

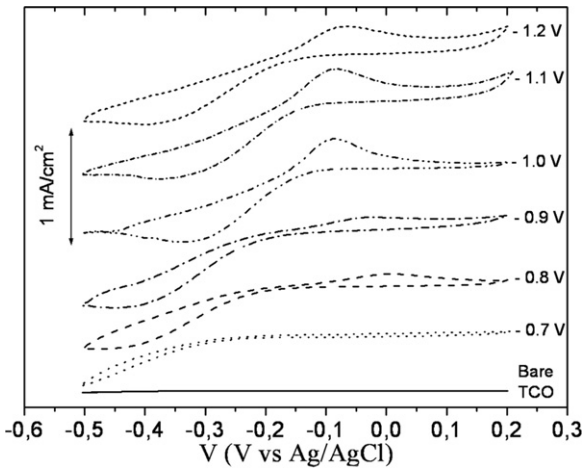

Figure 6. Cyclic voltammograms of the different gold surfaces in a KOH (0.5 M) aqueous solution saturated with oxygen.

orientation of the gold surface. Figure 6 shows the cyclic voltammetry (CV) curves obtained on gold surfaces of figure 1 in a 0.5 M of KOH aqueous solution saturated with O_2.

Different behaviours can be seen by comparing the different curves. No signal can be observed for the bare TCO substrate; hence, the signals at the other electrodes are considered to be from gold deposits. On the other hand, the catalytic peak current for the Au nanostructured electrodes (from −0.9 to −1.2 V) are much more enhanced than that for the compact Au layers (−0.7 and −0.8 V), showing that reduction reactions are more favourable at the larger surface area of nanostructured electrodes. Furthermore, the Au(111) surfaces favour the two-electron reduction of oxygen to hydrogen peroxide (equation (5)):

$$O_2 + 2H^+ + 2e^- \rightarrow H_2O_2. \quad (5)$$

By comparing our results obtained in figure 2 and the CV curves of figure 6, we can see that the reversibility of the oxygen reduction reaction follows the same behaviour as the crystallographic surface orientation. In other terms, the reaction is more and more reversible when the surface is richer in (111) facets. Consequently, the reversibility of this reaction (equation (5)) can be easily controlled by controlling the applied potential used for the deposition of gold.

As a second potential application, we studied the SERS response of the nanostructured gold surfaces [27, 28] in the presence of a test molecule, BCB. The SERS effect is an enhancement of the Raman scattering intensity of a compound, caused by an electromagnetic field increase due to the excitation of localized surface plasmons in metallic nanostructures [29].

Figure 7(a) shows the Raman spectrum of BCB recorded on the sample prepared at −0.7 V. The strongest peak is located at ∼590 cm^{-1}, as expected for BCB [30]. In figure 7(b), the intensity of the Raman signal (blue dots, left axis) is plotted against the deposition voltage, together with the roughness measured by AFM (red squares, right axis). The Raman intensity first decreases from −0.7 to −0.8 V, then increases again and reaches a plateau at −1.0 V, before decreasing again at −1.2 V, clearly indicating a dependence of the gold nanostructures. In fact, when the surface becomes rougher, the SERS enhancement is favoured: it is well known that junctions between adjacent nanoparticles possess highly SERS-active sites, due to the existence of so-called 'hot-spots', where intense local electromagnetic fields occur in the gaps and where highly efficient Raman scattering is found [10, 31].

By comparing the SERS efficiency of the samples at different deposition voltages with the roughness measured by AFM in figure 7(b), a very clear correlation is observed up to −1.0 V; after that, the roughness continues to increase, but the SERS efficiency does not. This is due to the size of the pyramidal-shaped nanostructures: the SERS effect is a near-field phenomenon which requires subwavelength sizes in order to efficiently couple the light with the localized surface plasmons. When the surface crystals get too big, they can be less excited by the laser light and in turn enhance less the Raman signal of the deposited BCB [18]. At −1.2 V for instance, the surface crystals are approaching 1 μm (see figure 1(f)). Therefore, the evolution of the SERS effect with the deposition voltage can be explained by the competition between the generation of hot-spots (which follows the

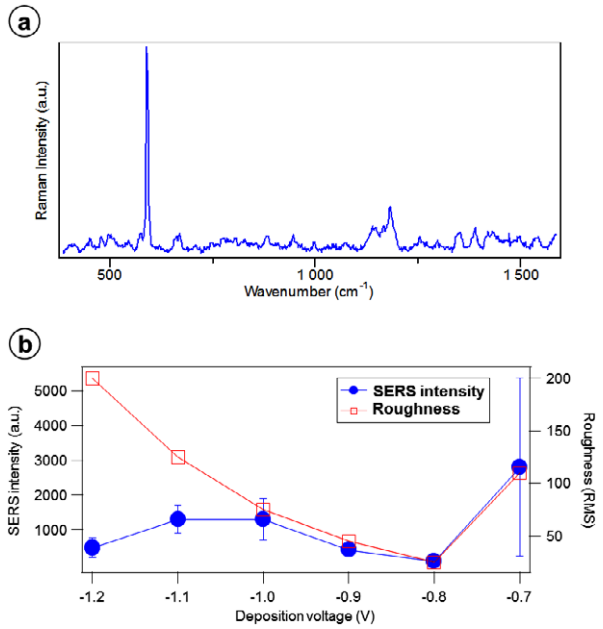

Figure 7. (a) Raman spectrum of BCB deposited on a gold surface and (b) evolution of SERS intensity and roughness with the deposition voltage.

roughness) and the size of the nanostructures (which increases continuously from −1.0 to −1.2 V).

4. Conclusions

In summary, gold thin layers with well-controlled roughness, morphology and crystallographic orientation have been synthesized by a simple and relatively low temperature electrochemical deposition method. The applied deposition potential played a major role in controlling these different factors (roughness, morphology and crystallographic orientation). The nucleation and the growth process have been investigated by electrochemical characterization and a formation mechanism has been proposed. As a first application, the different gold deposits with different geometries and orientations have shown a clear correlation with the electrocatalytical activity in the case of oxygen sensing. Furthermore, the SERS activity of the gold deposits has been found to depend both on the roughness and on the size of the surface nanostructures, allowing a fine tuning by controlling these two parameters during deposition. Future work will investigate the possible use of these substrates for applications in sensors and superhydrophobic surfaces.

Acknowledgments

This work was supported by the NanoGold project, Switzerland and partially funded by COST action MP0701 nanocomposite materials.

References

[1] Link S and El-Sayed M A 1999 *J. Phys. Chem.* B **103** 8410
[2] Kolb D M 2001 *Angew. Chem. Int. Edn* **40** 1162
[3] Fernandez E M, Soler J M, Garzon I L and Balbas L C 2004 *Phys. Rev.* B **70** 165403
[4] Dawson A and Kamat P V 2001 *J. Phys. Chem.* B **105** 960
[5] Elghanian R, Storhoff J J, Mucic R C, Letsinger R L and Mirkin C A 1997 *Science* **277** 1078
[6] Kneipp K, Wang Y, Kneipp H, Perelman L T, Itzkan I, Dasari R and Feld M S 1997 *Phys. Rev. Lett.* **78** 1667
[7] Yu X, Wang Z Q, Jiang Y G, Shi F and Zhang X 2005 *Adv. Mater.* **17** 1289
[8] Haruta M 1997 *Catal. Today* **36** 153
[9] Mirkin C A, Letsinger R L, Mucic R C and Storhoff J J 1996 *Nature* **382** 607
[10] Bechelany M, Brodard P, Elias J, Brioude A, Michler J and Philippe L 2010 *Langmuir* **26** 14364
[11] Bond G C and Thompson D T 1999 *Catal. Rev. Sci. Eng.* **41** 319
[12] Dimitrov A S and Nagayama K 1996 *Langmuir* **12** 1303
Lyons P E, De S, Elias J, Schamel M, Philippe L, Bellew A T, Boand J J and Coleman J N 2011 *J. Phys. Chem. Lett.* **2** 3058
[13] Andersen H H and Bay H L 1975 *J. Appl. Phys.* **46** 2416
[14] Fan H Y, Yang K, Boye D M, Sigmon T, Malloy K J, Xu H F, Lopez G P and Brinker C J 2004 *Science* **204** 567
[15] Wu Z H, Mei X Y, Kim D, Blumin M and Ruda H E 2002 *Appl. Phys. Lett.* **81** 5177
[16] El-Deab M, Sotomura T and Ohsakaa T 2005 *J. Electrochem. Soc.* **152** C730
[17] Tian Y, Liu H, Zhao G and Tatsuma T 2006 *J. Phys. Chem.* B **110** 23478
[18] Elias J, Brodard P, Vernooij M G C, Michler J and Philippe L 2011 *Electrochim. Acta* **56** 1485
[19] Kim J, Huang X and Choi Y 2008 *J. Phys. Chem.* C **112** 12747
[20] Horcas I, Fernández R, Gómez-Rodríguez J M, Colchero J, Gómez-Herrero J and Baro A M 2001 *Rev. Sci. Instrum.* **78** 013705
[21] Praiga V G, Piret G, Manessea M, Castel X, Boukherroubb R and Szunerits S 2008 *Electrochim. Acta* **53** 7838
[22] Welinder A C, Zhang J D, Steensgaard D B and Ulstrup J 2010 *Phys. Chem. Chem. Phys.* **12** 9999
[23] Li Y G and Lasia A 1997 *J. Appl. Electrochem.* **27** 643
[24] Bindra P, Light D, Freudenthal P and Smith D 1989 *J. Electrochem. Soc.* **136** 3616
[25] Santinacci L, Djenizian T, Schwaller P, Suter T, Etcheberry A and Schmuki P 2008 *J. Phys. D: Appl. Phys.* **41** 175301
[26] Burda C, Chen X, Narayanan R and El-Sayed M A 2005 *Chem. Rev.* **105** 1025
[27] Bozzini B, Busson B, De Gaudenzi G P, D'Urzo L, Mele C and Tadjeddine A 2007 *J. Electroanal. Chem.* **602** 61
[28] Bozzini B, D'Urzo L, Mele C and Romanello V 2008 *J. Phys. Chem.* C **112** 6352
[29] Le Ru E C and Etchegoin P G 2009 *Principles of Surface-enhanced Raman Spectroscopy and Related Plasmonic Effects* (Amsterdam: Elsevier)
[30] Kim J H, Kang T, Yoo S M, Lee S Y, Kim B and Choi Y K 2009 *Nanotechnology* **20** 235302
[31] Bechelany M, Brodard P, Philippe L and Michler J 2009 *Nanotechnology* **20** 455302